

Effective Interfacial Thickness in Dissimilar Materials through Nanoindentation

S. S. Pulla¹ and Y. C. Lu¹

Abstract: The nanoindentation technique is used to quantify the interfaces between dissimilar materials. The interfaces can be generally referred as to the transition regions in polymers due to environmental aging, or the regions between fibers and polymer matrix in composites, or other similar situations. It is proposed to use a nanoindenter equipped with small spherical tip to cross-indent the interfaces of dissimilar materials. The nanoindentation tests were carried out through 3-dimensional finite element simulations with varying properties of the two dissimilar materials, including various combinations of modulus (E_1/E_2), yield strength (σ_{y1}/σ_{y2}), hardening index (n_1/n_2), and the interface sizes (R/T). The mechanical properties are calculated across the interfaces and a quantitative model for predicting the effective interfacial thickness is established.

Keywords: Nanoindentation; Interfacial thickness; Finite element method.

1 Introduction

The interface can be broadly defined as a region that separates two dissimilar materials. It can be generally referred as to the transition regions in polymers due to environmental aging, or the regions between hard fibers and soft polymer matrix in composites, or other similar situations. For example, at elevated temperatures, polymer resins are known to undergo thermo-oxidative aging (Schoeppner et al, 2007). As a result, the materials will change in both microstructure and mechanical properties, as characterized by the three-zone model: oxidized surface, unoxidized interior, and the interface (Tandon et al, 2002; Lu et al, 2009). Quantitative identification of the interfaces is critical in predicting the damage and lifetimes of the polymers and their composites (Schoeppner and Curliss, 2002). The identifications of the interfaces have been mostly achieved through various optical techniques, such as dark-field imaging (Broecket, 2007), polarized light microscopy (Schoeppner et al, 2007), and scanning electron microscopy (SEM)/ transmission electron

¹ Dept of Mechanical Engineering, University of Kentucky, Lexington, KY, U.S.A

microscopy (TEM) (Meador et al, 1996; Chaffin et al, 2000). However, with optical methods, the interfaces in some polymer systems can be easily identified and measured while the interfaces in other cases are completely invisible (Ripberger et al, 2005). Thus, new technique for measuring the interfaces is needed.

Interface study has also been a very important subject in fiber-reinforced polymer composites. The interfaces between reinforcing fibers and matrix play an important role in the overall performances of composites, particularly nanocomposites (Odegard, 2005). However, due to the small size, typically in the orders of nanometers or microns, it is often difficult to quantify the size of the interfaces (Kim and Mai, 1993; Lee et al, 2007; Wang and Hahn, 2007).

This paper presents the use of nanoindentation technique to quantify the interfaces between dissimilar materials. Nanoindentation test has become a well-recognized method for measuring the mechanical properties of materials in localized regions or in submicron dimensions. It employs high-resolution actuators and sensors to continuously control and monitor the loads and displacements on an indenter as it is driven into and withdrawn from a material. From the load-depth curve, the conventional mechanical properties such as modulus and hardness can be extracted (Oliver and Pharr, 1992, 2004, Doerner and Nix, 1986). However, the nanoindentation technique has so far been limited to measuring the mechanical properties. The present work is to use nanoindentation to study the interface of dissimilar materials, with the goals of both extracting mechanical properties and estimating the effective thickness of the interfaces. Three-dimensional finite element modeling will be conducted since the dissimilar materials are heterogeneous structures.

2 Procedures of 3D Finite Element Simulations

The interface can represent the region between oxidized and unoxidized polymer resins or the region between rigid fiber and polymer matrix. A general interface model can be sketched as seen in Figure 1. The dissimilar material consisted of three distinct regions: region one made of material I, interface, and region two made of material II. To evaluate the properties and effective thickness of the interface, a series of indentation tests were conducted with the small indenter along the surface of the specimen. In many applications, the thickness of the interfaces could be as small as a few nanometers (nm). Therefore, the interfaces could not be directly measured even with the smallest indenter. It was proposed to use a sharp indenter with a rounded tip (spherical shape), whose size (radius R) could be even bigger than the interface, to obtain the average properties of the interface. The normalized interfacial thickness was ranged as $T/R = 0, 0.25, 1, 2$, where T is the interface thickness and R the indenter tip radius.

The general purpose finite element program, ABAQUS (Dassault Systèmes Simulia Corp. Providence, RI) (ABAQUS, 2010), was used for the simulations. The structure was modeled with the three-dimensional element, C3D8R, and the indenter was modeled as a rigid surface. Frictional contact was assumed between the indenter and specimen. The materials were treated as elastic-plastic defined by a piecewise linear/power-law hardening relation:

$$\sigma = \begin{cases} E\varepsilon & \text{for } \sigma \leq \sigma_y \\ \sigma_y \left(\frac{\varepsilon}{\varepsilon_y}\right)^n & \text{for } \sigma > \sigma_y \end{cases} \quad (1)$$

where “ σ ” and “ ε ” were the applied stress and strain; “ σ_y ” and “ ε_y ” the material yield stress and strain (assuming the material was linear elastic to the yield point); “ E ” the Young’s modulus; and “ n ” the strain hardening exponent describing the post-yield material behavior as a power law relation. The plasticity was modeled by a standard von Mises (J_2) flow criterion (Dassault Systèmes Simulia Corp. Providence, RI) (ABAQUS, 2010).

The material properties at region II were fixed: $E_2=1200$ MPa, $\sigma_{y2}=59$ MPa, $n_2=0.5$, and $\nu=0.33$. The material properties at region I were varied, including various combinations of E_1/E_2 (varied from 1, 1.5, 2, 2.5, 3, 3.5, 4), σ_{y1}/σ_{y2} (varied from 1, 1.5, 2, 2.5, 3, 3.5, 4), and $n_1=n_2$ (0.5, 0.4). The Poisson’s ratio was set to 0.33 for both materials. For each case, an average of 12 indents was conducted across the interface. A total of over 1000 indentation tests were conducted.

3 Results and Discussion

3.1 Nanoindentation of Homogeneous Materials

To validate the elastic-plastic finite element model, the indentation tests were first performed on homogeneous materials (region I, region II, and interface were assigned the same material properties in the model). A range of materials with known modulus ($E=1020\sim 5010$ MPa) were tested and the indentation load-depth curves obtained (Figure 2). The procedures for analyzing nanoindentation experiments on homogeneous materials have been well established, as follow (Oliver and Pharr, 1992, 2004):

The elastic contact stiffness, S , is estimated from the slope of the initial portion of the unloading curve

$$S = dP/dh \quad (2)$$

where P is the load and h is the displacement at the indenter tip.

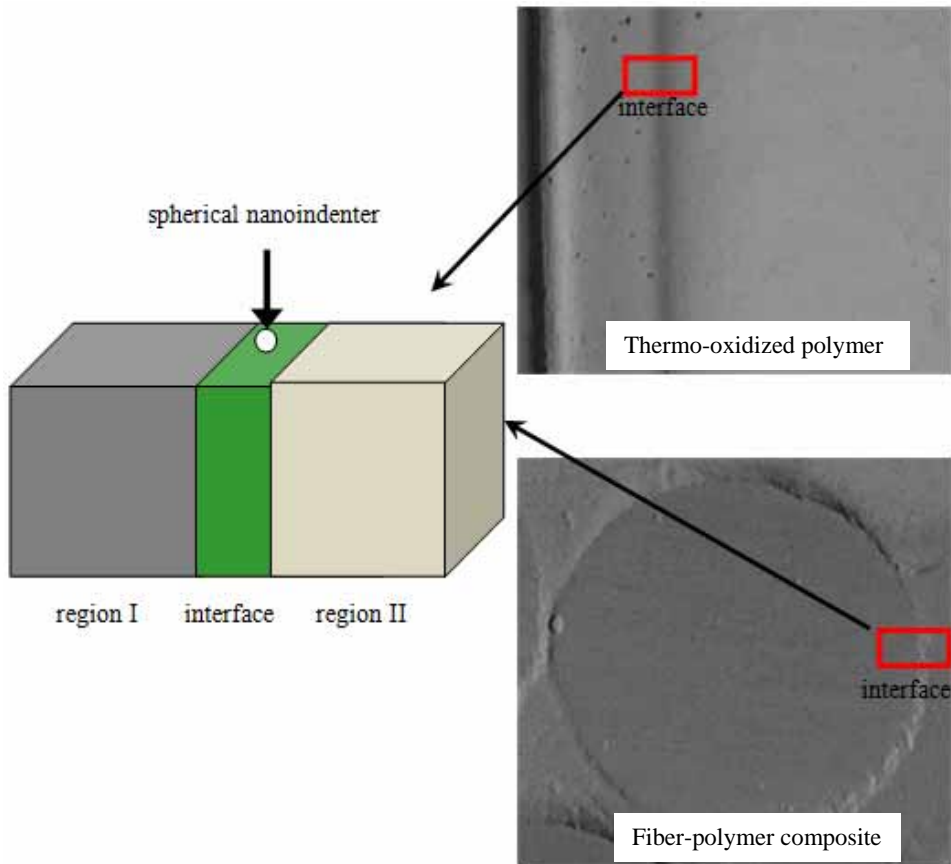


Figure 1: A generic model representing the interface of dissimilar materials.

Due to material sink-in around the indenter, the actual contact depth, h_c , is determined from the loading-unloading curve

$$h_c = h - 0.75P/S, \quad (3)$$

where h is the total indentation depth and P the maximum load.

The indenter-sample contact radius (a) is then computed via the standard procedure

$$E^* = \frac{1}{\beta} \frac{\sqrt{\pi}}{2} \frac{S}{\sqrt{A}} \quad (4)$$

The projected contact area, A , can be estimated through the impression radius a

$$A = \pi a^2 \tag{5}$$

Once the contact area is determined the hardness and reduced modulus and can be calculated as:

$$\frac{1}{E_r} = \frac{1 - \nu_1^2}{E_1} + \frac{1 - \nu_2^2}{E_2} \tag{6}$$

$$H = P/A \tag{7}$$

where $E^* = \frac{1}{\beta} \frac{\sqrt{\pi}}{2} \frac{S}{\sqrt{A}}$. E_i and ν_i are the elastic modulus and Poisson’s ratio of the indenter (for diamond indenter: $E_i=1140$ GPa and $\nu=0.07$, Oliver and Pharr, 1992, 2004).

Based upon the information obtained from the load-depth curves (Figure 2), the modulus of each material is extracted by using Equation 6. A comparison of modulus from indentation tests and the given values is shown in Figure 3. It is seen that the results from indentation tests agree well with the input values, with an error less than 5%. This indicates that the present elastic-plastic FE model is appropriate for studying the interface problems.

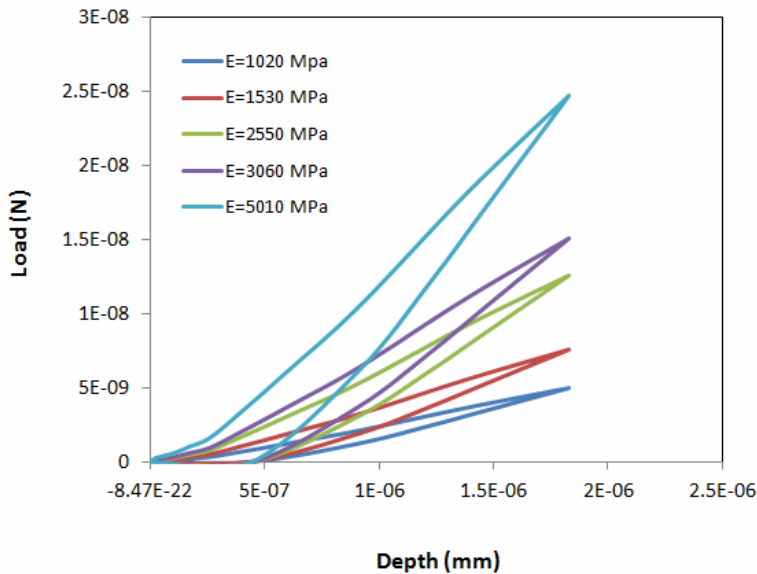


Figure 2: Indentation load-depth curves of homogeneous materials

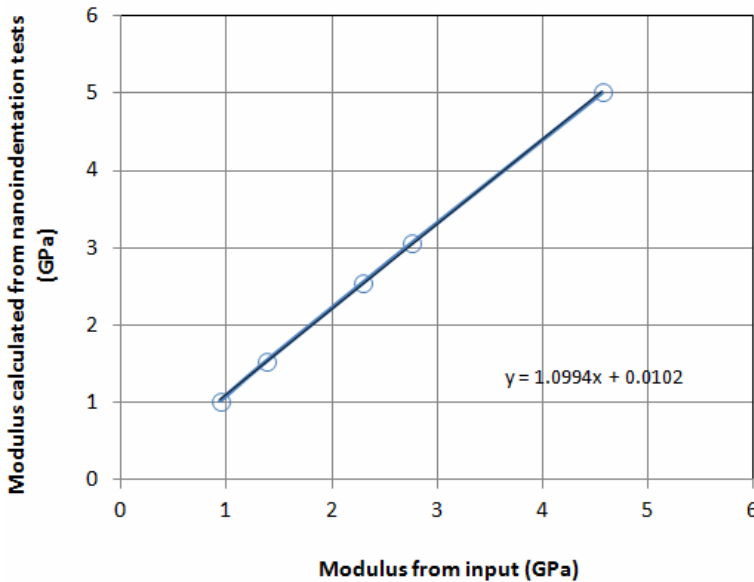


Figure 3: Comparison of modulus from indentation tests and input values for a variety of homogeneous materials.

3.2 Nanoindentation of the Interfaces

The same FE model was then partitioned into three different regions, including an interface, and indentation tests were performed across the interface. Figure 4 shows the distributions of von Mises stress (σ_{Mises}) at the different positions for a given set of material properties: $E_1/E_2=3$, $R/T=0.25$, $n_1=n_2=0.5$. At positions far away from the interface, the materials are essentially homogeneous and thus the von Mises contours are seen to be continuous and not affected by the presence of the interface. Near or inside the interface, the von Mises contours are discontinuous indicating that the material in the interface region is highly inhomogeneous.

Figure 5 shows the contours of von Mises at the center of the interface for different modulus ratios: $E_1/E_2=1.0\sim 4$. It is seen that the stress distributions within the interface are strongly affected by the moduli of surrounding bulk materials. Higher modulus ratio results in higher irregularity of the stress trajectories.

As shown in the von Mises contours (Figures 4 and 5), the interfaces are inhomogeneous structure, thus the conventional procedures for calculating stiffness and modulus from indentation tests (Equations 2 and 6) are in fact invalid. However, the results can still be used to show the variations of properties at the interfaces.

Figure 6 shows the indentation load-depth responses across the interface for the case of $E_1/E_2=2.5$, $R/T=2$. From the load-depth curves, the modulus and hardness across the interfaces are computed by using Equations 6 and 7, respectively. Figures 7-8 show the variations of modulus and hardness across the interface for the case of $E_1/E_2=2.5$, $R/T=2$. All results have clearly demonstrated the existences of three regions in the materials: material I, the interface, and materials II. Material I and material II are the regions that are far away from the interface and thus can be considered as homogeneous. The moduli of these two regions correspond to the values as obtained from testing homogeneous materials (Figure 3). Within the transition regions (interfaces), the moduli decrease progressively. For all the structures analyzed, material II (the left region) has varying properties while material I (the right region) has the fixed properties. As the indenter moved from material I to material II in each sample, it is seen that the modulus values tend to be close to each other and reach a constant value.

3.3 Effective Interfacial Thickness

Although nanoindentation has been widely used to measure the mechanical properties of materials and structures in small dimensions, it has yet been used to explore its other potentials. The objective of the present study is to use nanoindentation to estimate the effective thickness at the interfaces, where the traditional optical methods become invalid. A numerical method for estimating the interface thickness has been recently proposed by Yang et al (Yang et al 2009). However, the analysis is based upon a 2D wedge indentation model, which does not accurately represent a 3D spherical indenter.

In the present study, the spherical indentation was treated by a three-dimensional (3D) finite element model. Based on the hardness data across the interfaces (Figure 8), the apparent interfacial thickness (width), W , is calculated (Yang et al 2009):

$$W = \frac{H_1 - H_2}{|k|} \quad (8)$$

where H_1 and H_2 are the hardness of the two bulk materials, which are the hardness calculated from locations far away from the interface. Within the interface, the hardness values are seen to vary linearly and thus can be fit to straight lines, from which the slopes k are computed.

In the FE models, the true interfacial thickness (width), W_T , are known, so the relationship between apparent thickness (W) and true thickness (W_T) can be established, as shown in Figure 9. To make the results independent upon the indenter size, all values have been normalized with the indenter radius, R . It is seen that the relationships between apparent thickness (W) and true thickness (W_T) follow the

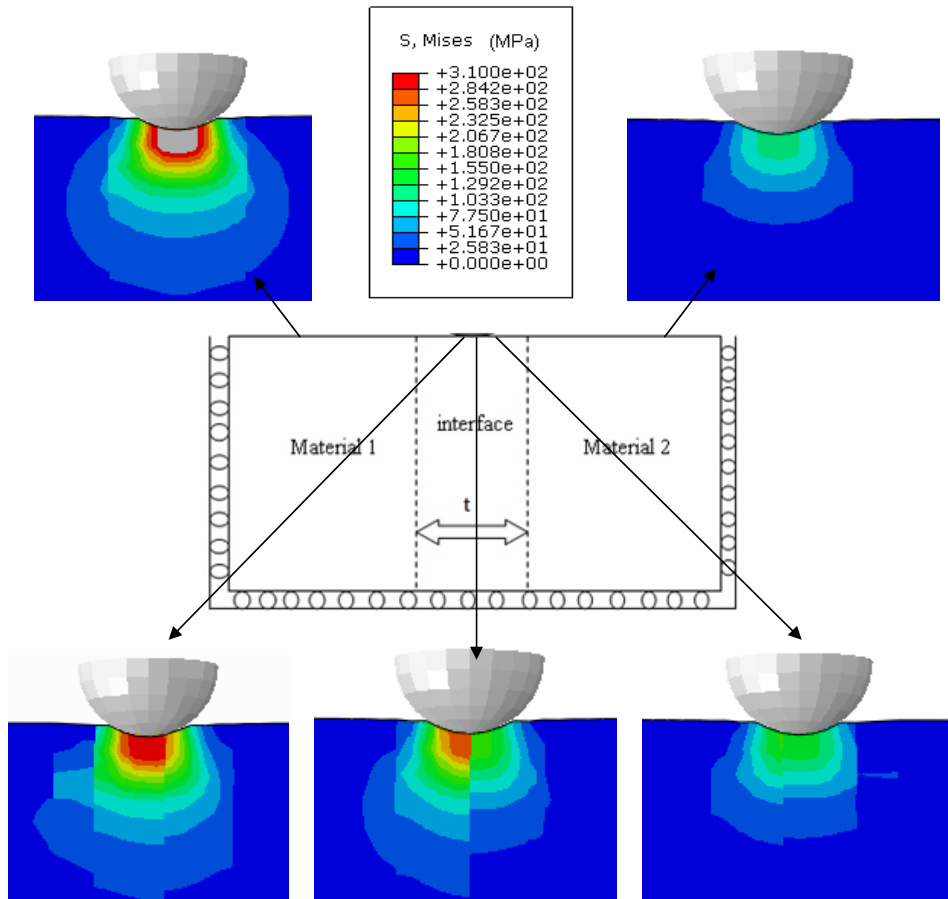
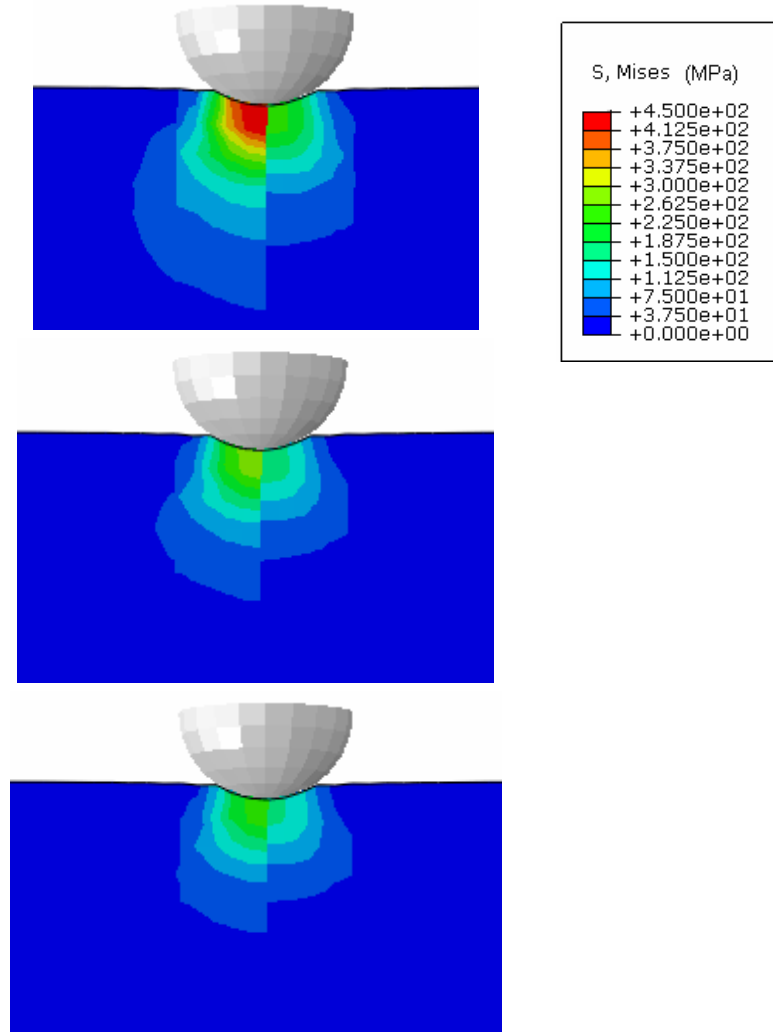


Figure 4: von Mises stress distribution across the interface for $E_1/E_2=3$ and $R/T = 0.25$.

same trend, in a simple linear function (Yang et al 2009):

$$\frac{W}{R} = \xi \frac{W_T}{R} + \frac{W_0}{R} \quad (9)$$

where ξ is the slope of each $W-W_T$ curve corresponding to different material properties. The values of ξ are found to be identical regardless of the properties of the interfaces, with an average being: $\xi=0.92$. Although all curves have similar slopes,



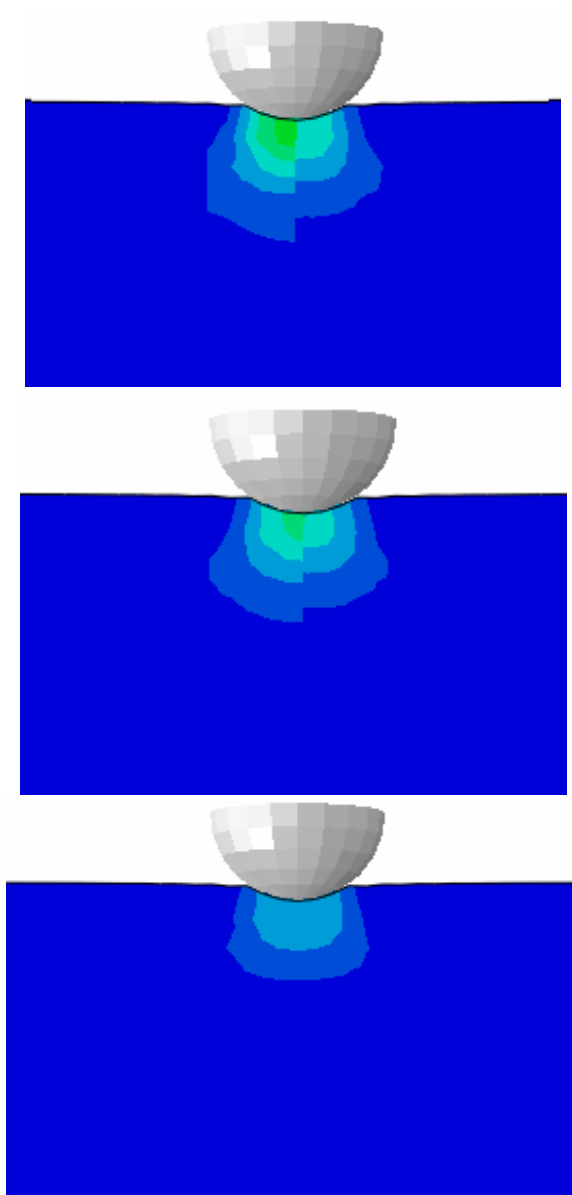


Figure 5: von Mises stress distribution at the interface: $R/T=0.25$, $E_1/E_2=4, 3, 2.5, 2, 1.5, 1$.

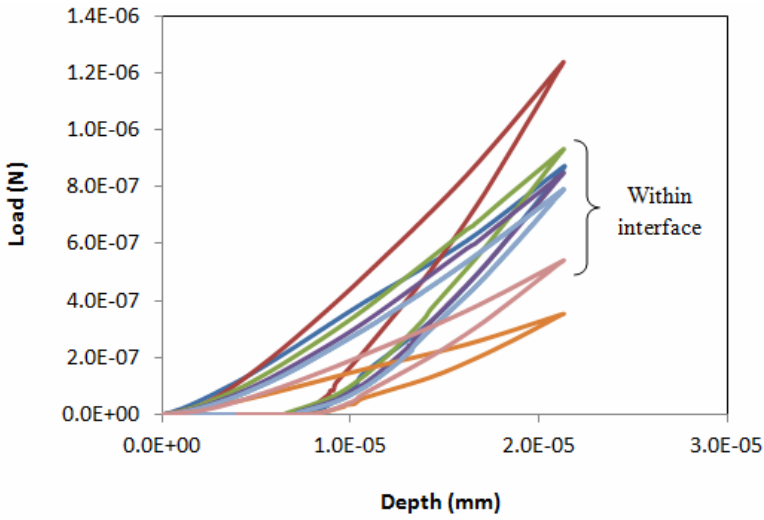


Figure 6: Indentation load-depth curves across the interface: $E_1/E_2=2.5$, $R/T=2$.

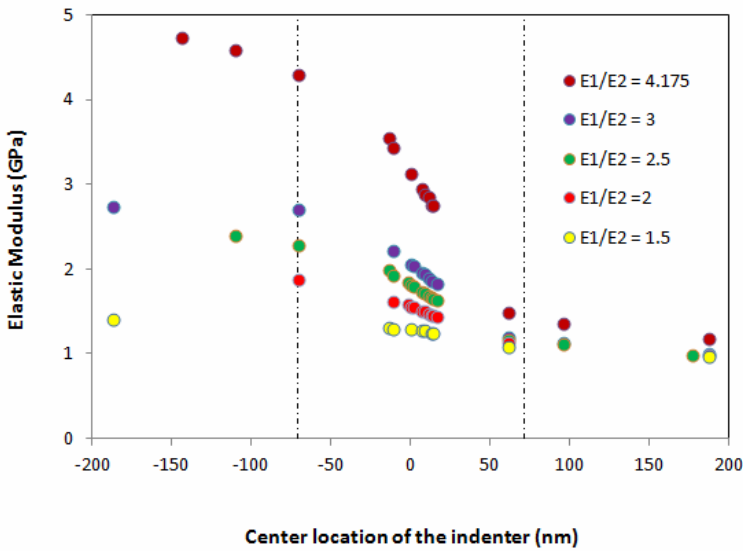


Figure 7: Modulus vs position across the interface: $R/T=2$. Dashed lines indicate the boundaries of the interface.

they have different intercepts (W_0). Here W_0 can be interpreted as an uncertainty term, whose magnitude depends upon the material properties of the materials sur-

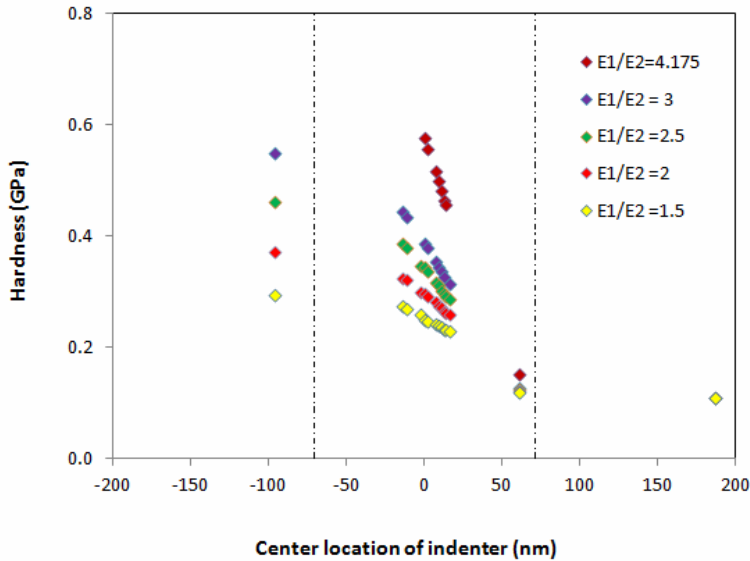


Figure 8: Hardness vs position across the interface: $R/T=2$. Dashed lines indicate the boundaries of the interface.

rounding the interfaces, and can be expressed as:

$$\frac{W_0}{R} = f\left(\frac{E_1}{E_2}, \frac{\sigma_{y1}}{\sigma_{y2}}, \frac{n_1}{n_2}, \frac{\nu_1}{\nu_2}\right) \quad (10)$$

where E , σ_y , n and ν are modulus, yield strength, strain hardening index and Poisson's ratio, respectively, and the subscripts, 1 and 2, refer to two bulk materials next to the interface. The Poisson's ratio has been found to have negligible effect on indentation responses, and can thus be ignored. Analyses have been carried out on materials with a wide range of properties. A plot of W_0 vs $\frac{E_1}{E_2} \frac{\sigma_{y1}}{\sigma_{y2}} \frac{n_1}{n_2} - 1$ is shown in Figure 10.

The data are seen to follow a power function:

$$\frac{W_0}{R} = \beta \left(\frac{E_1}{E_2} \frac{\sigma_{y1}}{\sigma_{y2}} \frac{n_1}{n_2} - 1 \right)^{-\alpha} \quad (11)$$

where the two coefficients are estimated as: $\alpha=0.28$ and $\beta=2.8$.

Combining Equations 9 and 11, the true interfacial thickness W_T for any unknown interface can then be estimated:

$$0.92 \frac{W_T}{R} = \frac{W}{R} - 2.8 \left(\frac{E_1}{E_2} \frac{\sigma_{y1}}{\sigma_{y2}} \frac{n_1}{n_2} - 1 \right)^{-0.29} \quad (12)$$

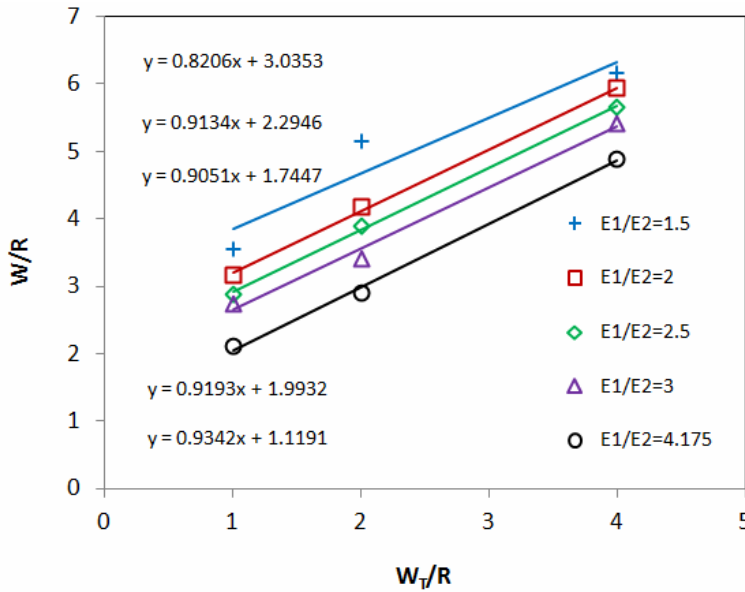


Figure 9: Plots of apparent interfacial thickness (W/R) and true interfacial thickness (W_T/R).

4 Summary

The identifications of the interfaces between dissimilar materials (such as the oxidized and unoxidized polymers or fibers and polymer matrix) have been mostly achieved through various optical techniques. However, in many cases the traditional optical methods fail to reveal the interfaces since the interfaces exhibit no visible differences from surrounding bulk materials. Furthermore, the traditional optical methods could not yield quantitative information about the properties of the interfaces. In this paper, the nanoindentation technique has been used to quantify the interfaces between dissimilar materials. It is proposed to use a small nanoindenter with rounded (spherical) tip to cross-indent the interfaces of dissimilar materials. The nanoindentation tests have been carried out through three-dimensional (3D) finite element simulations. Various interface scenarios have been modeled by varying the properties of the two dissimilar materials, including various combinations of modulus (E_1/E_2), yield strength (σ_{y1}/σ_{y2}), hardening index (n_1/n_2), and the interface sizes (R/T).

Results have shown that the stress distributions at the interfaces are strongly affected by the properties of the surrounding materials. By indenting across the interfaces, the mechanical properties (stiffness, modulus, and hardness) were calculated.

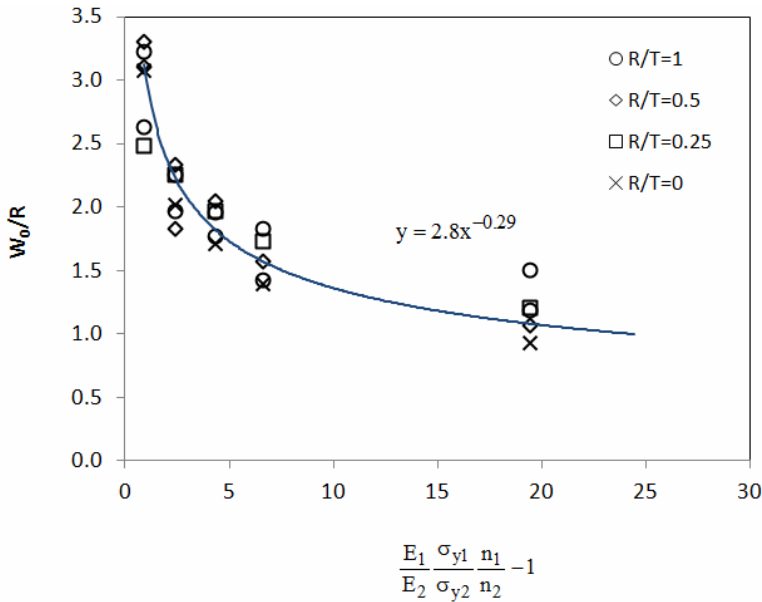


Figure 10: The generalized relation between interfacial thickness uncertainty (W_0/R) and material properties.

The mechanical properties at interfaces are seen to increase with the increase of modulus ratios E_1/E_2 , yield strength ratios σ_{y1}/σ_{y2} , and hardening index ratios n_1/n_2 , and with the decrease of interface size (R/T). By considering the hardness as the true properties of the interfaces, the apparent interfacial thickness (W) could be estimated from the nanoindentation tests. Finally, a quantitative equation for predicting the effective thickness of the interfaces (W_T) is established.

References

ABAQUS (2009) ABAQUS Users' Manual, Hibbit, Karlson and Sorenson Inc., Pawtucket, RI.

Chaffin, K.A., Bates, F.S., Brant, P., Brown, G.M. (2000) Semicrystalline blends of polyethylene and isotactic polypropylene: Improving mechanical performance by enhancing the interfacial structure. *J. Polym. Sci., Part B: Polym. Phys.* 38(1), 108.

Doerner, M.F., Nix, W.D. (1986) A method for interpreting the data from depth-sensing indentation instruments. *J. Mater. Res.* 4, pp. 601–609.

Kim, J.K., Mai, Y.W. (1993) Interfaces in Composites, In: Chou, T.W., Edi-

tor, *Materials Science and Technology: structure and properties of composites*, 13, Weinheim, Germany: p. 229-289.

Lee, S.-H., Wang, S., Pharr, G.M., Xu, H. (2007) Evaluation of interphase properties in a cellulose fiber-reinforced polypropylene composite by nanoindentation and finite element analysis, *Composites: Part A* 38, 1517-1524.

Lu, Y.C., Tandon, G. P., Jones, D.C., Schoeppner, G. A. (2009) Elastic and viscoelastic characterization of thermally-oxidized polymer resin using nanoindentation, *Journal of Mechanics of Time-Dependent Materials*, 13: 245–260.

Meador, M. A. B., Lowell, C. E., Cavano, P. J., and Herrera-Fierro, P. (1996) On the Oxidative Degradation of Nadic Endcapped Polyimides: I. Effect of Thermocycling on Weight Loss and Crack Formation, *High Performance Polymers*, 8, 363.

Odegard, G.M., Clancy, T.C., Gates, T.S.(2005) Modeling of the Mechanical Properties of Nanoparticle/Polymer Composites, *Polymer*, Vol. 46, no. 2, pp.553-562.

Oliver, W.C., Pharr, G.M. (1992) An improved technique for determining hardness and elastic modulus using load and displacement sensing indentation experiments, *Journal of Materials Research*, 7, 1564.

Oliver, W. C., Pharr, G. M., (2004) Measurement of hardness and elastic modulus by instrumented indentation: Advances in understanding and refinements to methodology, *Journal of Materials Research*, Vol. 19, pp. 3-20.

Ripberger E. R., Tandon, G. P., Schoeppner, G. A. (2005) Experimental Techniques for Characterizing Thermo-Oxidative Behavior in High-Temperature Polyimide Composites, Proceeding of SEM Annual Conference & Exposition on Experimental and Applied Mechanics.

Schoeppner, G.A., Curliss, D.B. (2002) Model-based design for composite materials life management, in 9th AIAA/ISSMO Symposium on Multidisciplinary Analysis and Optimization, Atlanta,GA.

Schoeppner, G. A., Tandon, G. P., Pochiraju, K. V. (2007) Predicting Thermo-Oxidative Degradation and Performance of High Temperature Polymer Matrix Composites, in *Multiscale Modeling and Simulation of Composite Materials and Structures*, s.l: Springer, pp 359-462.

Tandon, G. P., Pochiraju, K. V., Schoeppner, G. A. (2006) Modeling of oxidative development in PMR-15 resin, *Polymer Degradation and Stability*, vol. 91, no. 8, pp. 1861-1869.

Wang, Y., Hahn, T.H. (2007) AFM characterization of the interfacial properties of carbon fiber reinforced polymer Composites subjected to hygrothermal treatments,

Composites Science and Technology 67, 92-101.

Yang, C., Lo, C-T., Bastawros, A.F., Narasimhan, B. (2009) Measurements of diffusion thickness at polymer interfaces by nanoindentation: A numerically calibrated experimental approach”, *J. Mater. Res.*, Vol. 24, No. 3.